

Possible evidence for a variable fine structure constant from QSO absorption lines: motivations, analysis and results[☆]

M. T. Murphy¹, J. K. Webb^{1†}, V. V. Flambaum¹, V. A. Dzuba¹,
 C. W. Churchill², J. X. Prochaska³, J. D. Barrow⁴ and A. M. Wolfe⁵

¹*School of Physics, The University of New South Wales, UNSW Sydney NSW 2052, Australia*

²*Department of Astronomy & Astrophysics, Pennsylvania State University, University Park, PA, 16802, USA*

³*The Observatories of the Carnegie Institute of Washington, 813 Santa Barbara St. Pasadena, CA 91101*

⁴*Department of Applied Mathematics and Theoretical Physics, Centre for Mathematical Sciences, University of Cambridge, Wilberforce Road, Cambridge CB3 0WA, England, UK*

⁵*Department of Physics and Center for Astrophysics and Space Sciences, University of California, San Diego, C-0424, La Jolla, CA 920923*

Accepted —. Received —; in original form —

ABSTRACT

An experimental search for variation in the fundamental coupling constants is strongly motivated by modern high-energy physics theories. Comparison of quasar absorption line spectra with laboratory spectra provides a sensitive probe for variability of the fine structure constant, α , over cosmological time-scales. We have previously developed and applied a new method providing an order of magnitude gain in precision over previous optical astrophysical constraints. Here we extend that work by including new quasar spectra of damped Lyman- α absorption systems. We also re-analyse our previous lower redshift data and confirm our initial results. The constraints on α come from simultaneous fitting of absorption lines of subsets of the following species: Mg I, Mg II, Al II, Al III, Si II, Cr II, Fe II, Ni II and Zn II. We present a detailed description of our methods and results based on an analysis of 49 quasar absorption systems (towards 28 QSOs) covering the redshift range $0.5 < z < 3.5$. There is *statistical* evidence for a smaller α at earlier epochs: $\Delta\alpha/\alpha = (-0.72 \pm 0.18) \times 10^{-5}$. The new and original samples are *independent* but separately yield consistent and significant non-zero values of $\Delta\alpha/\alpha$. We summarise the results of a thorough investigation of systematic effects published in a companion paper. The value we quote above is the raw value, not corrected for any of these systematic effects. The only significant systematic effects so far identified, if removed from our data, would lead to a *more significant* deviation of $\Delta\alpha/\alpha$ from zero.

Key words: atomic data – line: profiles – methods: laboratory – techniques: spectroscopic – quasars: absorption lines – ultraviolet: general

1 INTRODUCTION

High resolution spectroscopy of QSO absorption systems provides a precise probe of fundamental physics. In pre-

[☆] Data presented herein were obtained at the W.M. Keck Observatory, which is operated as a scientific partnership among the California Institute of Technology, the University of California and the National Aeronautics and Space Administration. The Observatory was made possible by the generous financial support of the W.M. Keck Foundation.

[†] E-mail: jkw@bat.phys.unsw.edu.au (JKW)

vious papers (Dzuba, Flambaum & Webb 1999a,b; Webb et al. 1999, hereafter W99) we introduced and applied a new and highly sensitive method for constraining space-time variations of the fine structure constant, $\alpha \equiv \frac{e^2}{\hbar c}$. Using 30 Keck/HIRES absorption spectra containing Mg II and Fe II, we reported a tentative detection of a variation in α : $\Delta\alpha/\alpha = (-1.09 \pm 0.36) \times 10^{-5}$, where $\Delta\alpha/\alpha$ is defined as

$$\Delta\alpha/\alpha = (\alpha_z - \alpha_0)/\alpha_0, \quad (1)$$

α_0 is the present day value of α and α_z is the value at the absorption redshift, z . The absorption redshifts ranged from ~ 0.6 – 1.6 .

Here we continue this work, presenting new measurements of $\Delta\alpha/\alpha$ in high redshift damped Lyman- α systems (DLAs) over the range $0.9 < z < 3.5$, and a re-analysis of the W99 data set. Four papers present our new work on this subject. A brief summary of all results is given in Webb et al. (2001). The present paper provides a detailed description of our methods and results. A companion paper (Murphy et al. 2001b, hereafter M01b) presents a thorough examination of systematic effects. An additional paper (Murphy et al. 2001c) presents an analysis of a sample of Si IV QSO absorbers.

The present paper is organized as follows. Section 2 describes theoretical motivations for a search for varying α . In Section 3 we summarise previous experimental constraints on varying α . Section 4 presents the theoretical basis of the new method for determining $\Delta\alpha/\alpha$ using QSO absorbers. Section 5 describes the experimental components of our study: high-resolution QSO observations and precise laboratory rest wavelength measurements. In Section 6 we discuss our analysis technique in detail and present our results. For completeness we also summarise the systematic effects discussed in detail in M01b. Section 7 summarises our new results and outlines future work.

2 THEORETICAL BACKGROUND

2.1 Early historical interest

The constancy of the fundamental constants began to be questioned when Milne (1935, 1937) and Dirac (1937) suggested that the Newtonian gravitational constant, G , may vary in cosmological time. Milne proposed a gravitational theory in which different physical ‘clocks’ – ‘ticking’ according to different physical processes – ‘tick’ at different rates as time progresses. The possible consequences of this hypothesis for biological and geological history were seized upon by Haldane (1937a,b) to explain aspects of their discontinuous development, whereas Kothari (1938) and Chandrasekhar (1939) pointed out some astronomical consequences of Dirac’s ‘large numbers hypothesis’ which might permit it to be tested by observation. Dirac’s Large Numbers Hypothesis attracted considerable interest (e.g. Teller 1948; Dicke 1957, 1961; Barrow 1990; Barrow & Tipler 1996) and the desire to place his idea of varying G on a firmer theoretical footing led to the development of scalar-tensor generalisations of Einstein’s theory of general relativity in which the variation of G was described self-consistently by the propagation of a scalar field which also acted as a source of space-time curvature (Brans & Dicke 1961).

Jordan (1937, 1939) was the first to consider how Dirac’s hypothesis might be applied to forces other than gravity, but rejected the possibility of time variations in the weak interaction or the electron-proton mass ratio (Jordan 1937, 1939). Later, Gamow (1967) showed that geological problems caused by Dirac’s proposed variation in G that had been pointed out by Teller (1948) could be avoided by interpreting the large numbers hypothesis as requiring the time-variation of the charge on the electron, e , rather than G . Observational limits on possible variations of α or the weak and strong interactions were more restrictive than those on G although no self-consistent theory permitting

the variation of non-gravitational force constants was developed to make the observational limits rigorous. Landau (1955) proposed that variation in α could be connected to renormalization rules in quantum electrodynamics.

Current motivation for a search for a varying α comes from modern theories which attempt to unify gravity with other interactions.

2.2 Modern theoretical motivations for varying α

At present there are many theoretical motivations for a search for varying α . However, these theories, being relatively recent, may not be widely appreciated within the context of astronomical tests of their viability. We therefore summarise recent ideas below.

2.2.1 Multi-dimensional unification theories

One of the greatest challenges facing modern theoretical physics is the quantization of the gravitational interaction. Early attempts at creating such a unification were made using a geometrization in $(4 + D)$ -dimensional curved space-times in the spirit of the old Kaluza-Klein scenario to unite gravity and electromagnetism (Kaluza 1921; Klein 1926). Three-dimensional gauge couplings like α , α_{weak} , and α_{strong} then must vary as the inverse square of the mean scale of the extra dimensions. Thus, the evolution of the scale size of the extra dimensions is related to variability of the low-energy coupling constants in the 4-dimensional subspace in simple Kaluza-Klein and superstring theories.

Damour & Polyakov (1994) showed that cosmological variation in α may proceed at different rates at different points in space-time (see also Forgács & Horváth 1979; Barrow 1987; Li & Gott 1998). Various functional forms for time variation of α/G have been derived using Kaluza-Klein theory and the assumption of constant masses. Chodos & Detweiler (1980) find $\alpha/G \propto t$ and Freund (1982) finds $\alpha/G \propto t^{1/4}$. Wu & Wang (1986) have found that $\frac{\dot{\alpha}}{\alpha} \propto \frac{\dot{G}}{G} \sim -10^{-11 \pm 1} \text{yr}^{-1}$ where the proportionality constant is unknown. It is interesting to note that using a similar analysis to Wu & Wang, Maeda (1988) derived $\alpha \propto t^{-4/3}$.

Marciano (1984) discussed the self-consistency relations required if there are simultaneous variations of different constants in unified gauge theories. He also examined any possible non-monotonic variation in α with t , using the running coupling dependence of strong, weak, and electromagnetic interactions to produce self-consistent predictions for the simultaneous variation of more than one coupling or mass ratio. These were discussed in Drinkwater et al. (1998). Typically, variation in G and α could be linked by relations of the form $\frac{\Delta\alpha}{\alpha^2} \sim \frac{\Delta G}{G}$.

These features of extra dimensions mean that in all string theories (and M-theory, of which they are presumed to be limiting cases, Hořava & Witten 1996a,b), any extra dimensions of space need to be held static with high accuracy in order to avoid gross conflict with observation. In the currently popular scenarios for M-theory (e.g. Antoniadis et al. 1998; Arkani-Hamed, Dimopoulos & Dvali 1998; Randall & Sundrum 1999a,b), only the gravitational force is assumed to act in all (> 3) spatial dimensions (the ‘bulk’) whilst all other interactions act only in 3-dimensional space (the

‘brane’). Observations of the constancy of 3-dimensional non-gravitational constants governing the strengths of those interactions in three dimensions (like α) could therefore be of crucial importance in testing this theoretical scenario. The scale of the extra dimensions was until recently believed to be necessarily of order the Planck scale $\sim 10^{-33}$ cm but it is possible they could be as large as ~ 0.01 mm leading to large changes in the form of the Newtonian law of gravity on length scales below this distance. At present, this is consistent with all known experiments. The challenge of testing the law of gravity on sub-millimetre scales is considerable because other forces strongly dominate the effects of gravity on these scales.

2.2.2 Scalar Theories

The first self consistent theory of electromagnetism which incorporates varying α , and which reduces to Maxwell’s theory in the limit of constant α , was that developed by Bekenstein (1982). It introduces a scalar field whose variation in space and time produces effective variation in the electron charge (or, equivalently, the permittivity of free space). The form of the propagation equation for the evolution of the scalar field is strongly constrained by the natural requirements that it be second order, causal and linearly coupled to the matter density. This particular theory has been constrained by several astronomical observations (Livio & Stiavelli 1998) and used to illustrate consequences of space and time variations of constants (Barrow & O’Toole 2000).

The general structure of Bekenstein’s theory can also be applied to other couplings, and it has recently been used to investigate the problem of varying the strong coupling constant of QCD by Chamoun, Landau & Vucetich (2000). Bekenstein makes the simplifying assumption that the gravitational sector of the theory be unchanged from that of general relativity. This amounts to neglecting the contribution of the kinetic energy of the scalar field associated with α variation to the expansion dynamics of the universe. This defect can be avoided in other versions of this theory (Barrow & Magueijo 2000; Magueijo 2000). It should be emphasised that there is no single self-consistent theory incorporating varying α and theoretical limits need to be quoted in conjunction with the theoretical framework used to confront observational data. If different interactions are unified by electro-weak or grand unified theories then the ramifications of introducing varying α will be deeper and wider and a scalar theory would need to accommodate the effects of varying α on the other gauge couplings.

2.2.3 Varying speed of light theories

One appeal of varying speed of light theories is that they provide alternative potential solutions to a range of cosmological problems such as the flatness, horizon and monopole problems (Moffat 1993, 1998; Barrow & Magueijo 1999a,b; Albrecht & Magueijo 1999; Barrow 1999). Barrow & Magueijo (1998) have also expressed Bekenstein’s (1982) varying- c theory in terms of varying c .

Barrow & Magueijo (2000) developed a particular theory for varying c (or α) in which the stress contributed by the cosmological constant varies through the combination

Λc^2 . They also showed how the observed non-zero cosmological acceleration (Schmidt et al. 1998; Perlmutter et al. 1999) might be linked to a varying α . They examined a class of varying- c theories in which changes in c are driven by a scalar field which is coupled to the gravitational effect of pressure. Changes in c convert the Λ energy density into radiation, preventing Λ from dominating the universe in the radiation epoch. As pressureless matter begins to dominate, variations in c slow, and Λ begins to dominate. The very slow variation of the scalar field driving changes in c is like that of scalar fields in quintessence theories in the presence of perfect fluids. This type of theory allows the time variations in c or α to be $\sim 10^{-5} H_0$ at $z \sim 1$ and yet the associated Λ term can be dominant today and produce acceleration (the 10^{-5} factor is created naturally in this theory by the ratio of the radiation to matter density in the universe today). We therefore expect only very small residual variation in α in a Λ dominated universe. The existence of simple theories of this sort provides a strong motivation for studies like the present one.

2.2.4 Other theories

Several authors have suggested other motivations for varying α . For example, Hill & Ross (1988a,b) (see also Hill, Steinhardt & Turner 1990) have suggested that oscillatory variations in α might be expected if there exists a soft boson field that has electromagnetic couplings to either the Maxwell scalar, $F_{\mu\nu}F^{\mu\nu}$, or to the electron state, $\bar{\psi}_e\psi_e$. If the boson field has a mass m then the frequency of emission and absorption of radiation will vary with a frequency $\sim m^{-1}$. An oscillatory α might also be attributable to the decaying oscillations of a scalar field that couples to $F_{\mu\nu}F^{\mu\nu}$. Such a theory is allowed by enforcing an approximate global symmetry (Carroll 1998).

In summary, there is much current theoretical motivation for experimental searches for variability in α , particularly at medium to high redshifts. A detection of variation may allow us to probe the extra dimensions expected from many modern unified theories. A search for varying α provides an important tool for seeking out and constraining the form of new physics.

3 PREVIOUS EXPERIMENTAL WORK

3.1 Terrestrial and laboratory constraints

Direct laboratory measurements provide interesting constraints on a time-varying α . Prestage, Robert & Maleki (1995) introduced a new technique comparing the rates of clocks based on ultra-stable oscillators. Relativistic corrections are order $(Z_n\alpha)^2$ where Z_n is the atomic number or nuclear charge. By comparing the rates of two clocks based on different atoms (H-maser and Hg^+) over a 140 day period, they were able to constrain $|\dot{\alpha}/\alpha| \leq 3.7 \times 10^{-14} \text{ yr}^{-1}$ (i.e. $|\Delta\alpha/\alpha| \leq 1.4 \times 10^{-14}$).

Model dependent upper limits on any variation have been claimed from an analysis of the Oklo phenomenon – a natural nuclear fission reactor that operated in Gabon, West Africa, ~ 1.8 billion years ago. Shlyakhter (1976) originally

constrained the energy of the nuclear resonance level in the ^{150}Sm isotope and related this to upper bounds on $|\Delta\alpha/\alpha|$. Damour & Dyson (1996) have also analysed the problem with different model assumptions and claim $-0.9 \times 10^{-7} < \Delta\alpha/\alpha < 1.2 \times 10^{-7}$. Recently, Fujii et al. (2000) obtained somewhat tighter constraints using new samples from the Oklo reactor: $\Delta\alpha/\alpha = (-0.04 \pm 0.15) \times 10^{-7}$.

However, the Oklo limit corresponds to variations at very low ‘redshift’, $z \sim 0.1$, in a non-cosmological environment. In the absence of a detailed theory giving both time *and* space variations of α , it is dangerous to compare time variations in areas of different gravitational potential (Barrow & O’Toole 2000). Also, there are considerable uncertainties regarding the complicated Oklo environment and any limits on α derived from it can be weakened by allowing other interaction strengths and mass ratios to vary in time as well.

3.2 Constraints from QSO spectra

Savedoff (1956) first analysed doublet separations seen in galaxy emission spectra to constrain possible time variation of α . Absorption lines in intervening clouds along the line of sight to QSOs are substantially narrower than intrinsic emission lines and therefore provide a more precise probe of α . This prompted Bahcall, Sargent & Schmidt (1967) to use alkali-doublet spacings seen in the absorption spectra of QSOs to arrive at firm upper limits on any variation. The appeal of this method is the huge time span probed by high-redshift observations. Wolfe, Brown & Roberts (1976) first applied the alkali-doublet (AD) method to intervening Mg II absorption. Varshalovich, Panchuk & Ivanchik (1996) have used the AD method for many absorbers to obtain upper limits on any variation at redshifts $z \sim 2.8\text{--}3.1$: $\Delta\alpha/\alpha = (2 \pm 7) \times 10^{-5}$.

Varshalovich, Potekhin & Ivanchik (2000) have recently analysed 16 Si IV absorption systems (towards 6 QSOs) using the AD method. They find a mean $\Delta\alpha/\alpha = (-4.6 \pm 4.3 \pm 1.4) \times 10^{-5}$ using the Si IV laboratory wavelengths of Morton (1991). The systematic component to the error above (1.4×10^{-5}) allows for the relative uncertainties of the Si IV laboratory wavelengths. However, Griesmann & Kling (2000) have increased the absolute precision of these wavelengths and their new values indicate that the Varshalovich et al. (2000) result should be corrected by $\approx +11.3 \times 10^{-5}$ to $\Delta\alpha/\alpha \approx (+7 \pm 4) \times 10^{-5}$ suggesting that the systematic error component added by Varshalovich et al. was significantly underestimated.

In Murphy et al. (2001c) we have used the new Griesmann & Kling laboratory wavelengths to constrain $\Delta\alpha/\alpha$ using 21 Si IV doublets towards 8 QSOs. The spectral resolution and SNR are higher than for the Varshalovich et al. sample. This, and the higher precision laboratory wavelengths, provide a more stringent constraint of $\Delta\alpha/\alpha = (-0.5 \pm 1.3) \times 10^{-5}$. This result is nevertheless a factor of 7 less precise than the results we present in this paper, highlighting the strength of the methods we use.

The optical techniques above were based on the AD method: constraining α from the splitting of single ADs such as Si IV, C IV and Mg II. Very recently, however, Dzuba et al. (1999a) and W99 proposed a new method that allows *an order of magnitude increase in precision*. The method

is based on measuring the wavelength separation between the resonance transitions of *different ionic species* with no restriction on the multiplet to which the transitions belong. We outline this many-multiplet (MM) method and discuss its advantages in Section 4 of this paper.

Radio spectra of QSO absorption clouds also provide the opportunity for tightly constraining possible variations in the fundamental constants. Wolfe et al. (1976) demonstrated that combining optical resonance and H I 21 cm hyperfine absorption spectra could yield constraints on $\alpha^2 g_p \frac{m_e}{m_p}$. Here, g_p is the proton g-factor and m_e and m_p are the mass of the electron and proton respectively; see also the discussion by Pagel (1983). Varshalovich & Potekhin (1996) used a comparison of H I 21 cm hyperfine and molecular rotational absorption to constrain variations in m_p but Drinkwater et al. (1998) showed that such a combination actually constrains $y \equiv \alpha^2 g_p$. In Murphy et al. (2001d) we have also made a more complete analysis of the two Drinkwater et al. radio spectra to obtain constraints on y . Assuming g_p to be constant, we find $\Delta\alpha/\alpha = (-0.10 \pm 0.22) \times 10^{-5}$ and $\Delta\alpha/\alpha = (-0.08 \pm 0.27) \times 10^{-5}$ at $z = 0.25$ and 0.68 respectively. If we note the low- z points in the lower panel (binned data) of Fig. 3 then we see that our results are also consistent with the two radio points. Carilli et al. (2000) have also recently analysed independent spectra of these two QSOs and find an upper limit on any variation consistent with our measurements: $|\Delta\alpha/\alpha| < 0.85 \times 10^{-5}$ (again assuming g_p to be constant).

Cowie & Songaila (1995) have also obtained constraints at $z \approx 1.78$. They compare the observed frequencies of the H I 21 cm and UV C I absorption lines which are sensitive to variations in $g_p \alpha^2 \frac{m_e}{m_p}$. If one assumes that $g_p \frac{m_e}{m_p}$ is constant then their constraint corresponds to $\Delta\alpha/\alpha = (0.35 \pm 0.55) \times 10^{-5}$.

3.3 Early universe (CMB and BBN)

A smaller value of α in the past would change the ionization history of the universe, postponing the recombination of electrons and protons, i.e. last-scattering would occur at lower redshift. It would also alter the ratio of baryons to photons at last-scattering, leading to changes in both the amplitudes and positions of features in the cosmic microwave background power spectrum, primarily at angular scales $\lesssim 1^\circ$ (Hannestad 1999; Kaplinghat, Scherrer & Turner 1999; Avelino, Martins & Rocha 2000; Battye, Crittenden & Weller 2000; Kujat & Scherrer 2000).

Kolb, Perry & Walker (1986) have discussed how limits can be placed on $\Delta\alpha/\alpha$ at the time of nucleosynthesis (corresponding to a redshift $z \sim 10^8\text{--}10^9$) by assuming a simple scaling between the value of α and the neutron-proton mass difference. Using observations of the ^4He abundance they derive limits of $|\dot{\alpha}/\alpha| < 15 \times 10^{-15} h_{100} \text{ yr}^{-1}$, corresponding to $|\Delta\alpha/\alpha| < 9.9 \times 10^{-5}$.

Barrow (1987) and Campbell & Olive (1995) considered the simultaneous variation of weak, strong and electromagnetic couplings on primordial nucleosynthesis. However, these limits are beset by a crucial uncertainty as to the electromagnetic contributions to the neutron-proton mass difference. Much weaker limits are possible if attention is re-

stricted to the nuclear interaction effects on the nucleosynthesis of deuterium, helium-3, and lithium-7.

Bergström, Iguri & Rubinstein (1999) have re-examined all light elements up to ^7Li . By including elements heavier than ^4He they avoid the problem of the unknown electromagnetic contributions to the neutron-proton mass difference, and argue that a more realistic limit, given the present observational uncertainties in the light element abundances is more like 2×10^{-2} .

4 THEORETICAL BASIS OF THE MANY-MULTIPLER METHOD

The MM method allows an order of magnitude greater precision compared to the previous AD method. The full details behind this technique are presented in detail in Dzuba et al. (1999a,b, 2001) and W99 and so we present only the salient features here.

To explain the MM method, we begin with a simple analytic approach to estimate the relativistic effects in transition frequencies. If we consider a many-electron atom/ion then the relativistic correction, Δ , to the energy of the external electron can be written as

$$\Delta \propto (Z_n \alpha)^2 |E|^{3/2} \left[\frac{1}{j + 1/2} - C(j, l) \right], \quad (2)$$

where Z_n is the nuclear charge, E is the electron energy ($E < 0$, $|E|$ is the ionization potential) and j and l are the total and orbital electron angular momenta. The contribution to the relativistic correction from many-body effects is described by $C(j, l)$. For s and p orbitals, $C(j, l) \approx 0.6$ and is of similar magnitude for d orbitals. Equation 2 therefore provides a general strategy for probing the relativistic corrections in resonance transitions.

For example, consider comparison of the transition energies of two $s-p$ transitions, one in a light ion, the other in a heavy ion (i.e. low and high Z_n respectively). The Z_n^2 term dominates so the relativistic corrections to the transition energies will differ greatly. Thus, comparison of the spectra of light and heavy species is a sensitive probe of α .

As a further example, consider an $s-p$ and a $d-p$ transition in a heavy species. The corrections will be large in each case but will be of opposite sign since the many-body corrections, $C(j, l)$, begin to dominate with increasing j . This situation also allows tight constraints to be placed on α .

Thus, comparing spectra of transitions from different multiplets and different atoms or ions, provides a sensitive method for probing variations in α . In comparison, the fine splitting of an $s-p$ doublet will be substantially smaller than the absolute shift in the $s-p$ transition energy since the excited p electron, with relatively small $|E|$, will have much smaller relativistic corrections than the s electron. Therefore, the AD method is relatively insensitive to variations in α .

More formally, the energy equation for a transition from the ground state, within a particular multiplet, at a redshift z can be written as

$$E_z = E_c + Q_1 Z_n^2 \left[\left(\frac{\alpha_z}{\alpha_0} \right)^2 - 1 \right] + K_1(\mathbf{L}, \mathbf{S}) Z_n^2 \left(\frac{\alpha_z}{\alpha_0} \right)^2 + K_2(\mathbf{L}, \mathbf{S})^2 Z_n^4 \left(\frac{\alpha_z}{\alpha_0} \right)^4, \quad (3)$$

where α_z may or may not be equal to the laboratory value, α_0 . Here, \mathbf{L} and \mathbf{S} are the electron total orbital angular momentum and total spin respectively and E_c is the energy of the configuration centre. Q_1 , K_1 and K_2 are relativistic coefficients which have been accurately computed in Dzuba et al. (1999a,b, 2001) using *ab initio* many-body calculations. These calculations were tested by comparison with experimental data for energy levels and fine structure intervals. Equation 3 forms the basis of the MM method since it can be applied to any resonance transition observed in the QSO spectra – another advantage it has over the AD method.

For our purposes, the most convenient form of equation 3 is written as

$$\omega_z = \omega_0 + q_1 x + q_2 y, \quad (4)$$

where ω_z is the wavenumber in the rest-frame of the cloud, at redshift z , ω_0 is the wavenumber as measured on Earth and x and y contain the information about a possible non-zero $\Delta\alpha/\alpha$:

$$x \equiv \left(\frac{\alpha_z}{\alpha_0} \right)^2 - 1 \quad \text{and} \quad y \equiv \left(\frac{\alpha_z}{\alpha_0} \right)^4 - 1. \quad (5)$$

The values of the relativistic corrections, q_1 and q_2 , are presented in Table 1 for all transitions commonly seen in optical QSO spectra. The values of the q_1 coefficients are typically an order of magnitude larger than the q_2 coefficients. Therefore, it is the relative magnitudes of q_1 for different transitions that characterize our ability to constrain $\Delta\alpha/\alpha$. The uncertainty in the q_1 coefficients varies from ion-to-ion and is $\sim 5 \text{ cm}^{-1}$ for alkali-like ions such as Mg II . However, the coefficients for the complicated Ni II transitions carry a larger uncertainty $\sim 200 \text{ cm}^{-1}$ (Dzuba et al. 2001). The form of equation 4 is very convenient since the second and third terms only contribute if $\Delta\alpha/\alpha \neq 0$: errors in the q_1 and q_2 coefficients cannot lead to an artificial non-zero value of $\Delta\alpha/\alpha$.

From equation 3 we can see that q_1 will be much larger in heavier ions due to the Z_n^2 dependence. Indeed, one can see in Table 1 several *combinations of transitions from different ions*, of very different mass, showing large differences between their respective q_1 coefficients. The combination of the $\text{Mg I } \lambda 2853$ line, the Mg II doublet and the five Fe II lines between $\lambda 2344$ and $\lambda 2600$ was used in W99 since the Fe II q_1 coefficients typically differ from those of the Mg lines by almost an order of magnitude. It is this comparison of spectra from different ions that allows the order of magnitude increase in precision over previous methods. For comparison, we present the line shifts in wavenumber, wavelength and velocity space arising from a shift of $\Delta\alpha/\alpha = +10^{-5}$ in Table 2.

Further examination of the q_1 coefficients in Table 1 reveals several other very useful combinations of lines. In particular, note the large *negative* values for the Cr II lines. A comparison between Cr II spectra and that of Zn II – the $\lambda 2026$ transition having the largest magnitude value of q_1 – provides the most sensitive combinations for probing non-zero $\Delta\alpha/\alpha$. Also, note the coefficients for Ni II . Here, within the same species (but different multiplets), we have both positive and negative values for q_1 . This unique case is due to the very complicated multiplet structure of Ni II as discussed in detail in Dzuba et al. (2001).

Table 1. Atomic data for those transitions used in our analysis. The origins of the composite wavenumbers (ω_0) and wavelengths (λ_0) are detailed in Section 5.2. We give the ground and excited state configurations in columns 4 and 5. The ID letters in column 6 are used in Table 4 to indicate the transitions used in our Voigt profile fits to each absorption system. The seventh column shows the ionization potential (IP)^a and the eighth shows the literature oscillator strengths, f . Values of q_1 and q_2 are also shown. The Si II, Al II and Al III wavenumbers have been scaled from their literature values due to the Norlén/Whaling et al. calibration difference described in Section 5.2. The isotopic structures for the Mg and Si transitions are given in Table 3.

Ion	λ_0 Å	ω_0 cm ⁻¹	Ground state	Upper state	ID	IP eV	f	q_1 cm ⁻¹	q_2 cm ⁻¹
Mg I	2852.96310(8)	35051.277(1) ^b	$3s^2\ ^1S_0$	$3s3p\ ^1P_1$	a	—	1.810 ^f	106	-10
Mg II	2796.3543(2)	35760.848(2) ^b	$3s\ ^2S_{1/2}$	$3p\ ^2P_{3/2}$	b	7.7	0.6295 ^g	211	0
	2803.5315(2)	35669.298(2) ^b		$3p\ ^2P_{1/2}$	c		0.3083 ^g	120	0
Al II	1670.7887(1)	59851.972(4) ^c	$3s^2\ ^1S_0$	$3s3p\ ^1P_1$	d	6.0	1.88 ^f	270	0
Al III	1854.71841(3)	53916.540(1) ^c	$3s\ ^2S_{1/2}$	$3p\ ^2P_{3/2}$	e	18.9	0.268 ^f	464	0
	1862.79126(7)	53682.880(2) ^c		$3p\ ^2P_{1/2}$	f		0.539 ^f	216	0
Si II	1526.70709(2)	65500.4492(7) ^c	$3s^23p\ ^2P_{1/2}^o$	$3s^24s\ ^2S_{1/2}$	g	8.2	0.116 ^h	24	22
	1808.01301(1)	55309.3365(4) ^c		$3s3p^2\ ^2D_{3/2}$	h		0.00218 ^f	525	3
Cr II	2056.25693(8)	48632.055(2) ^d	$3d^5\ ^6S_{5/2}$	$3d^44p\ ^6P_{7/2}$	i	6.8	0.105 ⁱ	-1030	-13
	2062.23610(8)	48491.053(2) ^d		$3d^44p\ ^6P_{5/2}$	j		0.078 ⁱ	-1168	-16
	2066.16403(8)	48398.868(2) ^d		$3d^44p\ ^6P_{3/2}$	k		0.0515 ⁱ	-1267	-9
Fe II	1608.45085(8)	62171.625(3) ^e	$3d^64s\ ^z6D_{9/2}$	$3d^64p\ ^y6P_{7/2}$	l	7.9	0.0619 ^j	1002	141
	1611.20034(8)	62065.528(3) ^e		$3d^64p\ ^y4F_{7/2}$	m		0.00102 ^j	1110	48
	2344.2130(1)	42658.2404(2) ^e		$3d^64p\ ^z6P_{7/2}$	n		0.110 ^j	1325	47
	2374.4603(1)	42114.8329(2) ^e		$3d^64p\ ^z4F_{9/2}$	o		0.0326 ^j	1730	26
	2382.7642(1)	41968.0642(2) ^e		$3d^64p\ ^z6F_{11/2}$	p		0.300 ^j	1580	29
	2586.6496(1)	38660.0494(2) ^e		$3d^64p\ ^z6D_o$	q		0.0684 ^j	1687	-36
	2600.1725(1)	38458.9871(2) ^e		$3d^64p\ ^4D_{9/2}$	r		0.213 ^j	1449	2
Ni II	1709.6042(1)	58493.071(4) ^d	$3d^9\ ^2D_{5/2}$	$3d^84p\ ^z2F_{5/2}$	s	7.6	0.0348 ^k	800	0
	1741.5531(1)	57420.013(4) ^d		$3d^84p\ ^z2D_{5/2}$	t		0.0419 ^k	-700	0
	1751.9157(1)	57080.373(4) ^d		$3d^84p\ ^z2F_{7/2}$	u		0.0264 ^k	-300	0
Zn II	2026.13709(8)	49355.002(2) ^d	$3d^{10}4s\ ^2S_{1/2}$	$3d^{10}4p\ ^2P_{3/2}$	v	9.4	0.489 ⁱ	2291	94
	2062.66045(9)	48481.077(2) ^d		$3d^{10}4p\ ^2P_{3/2}$	w		0.256 ⁱ	1445	66

^aIP is defined here to be the energy required to form the ion in question from the ion with a unit lower charge;

^bPickering, Thorne & Webb (1998); ^cGriesmann & Kling (2000); ^dPickering et al. (2000); ^eNave et al. (1991); ^fMorton (1991); ^gVerner, Verner & Ferland (1996); ^hDufton et al. (1983); ⁱBergeson & Lawler (1993); ^jCardelli & Savage (1995); ^kFedchak & Lawler (1999)

We may summarise the advantages of the MM method over the AD method as follows:

- By including *all* relativistic corrections (i.e. including those for the ground state) there is a sensitivity gain of around an order of magnitude compared to the AD method.
- In principle, all transitions appearing in a QSO absorption system may be used. This provides an obvious statistical gain and a more precise constraint on $\Delta\alpha/\alpha$ compared to using a single AD alone.
- A further advantage of using many transitions is that the velocity structure is determined with much greater reliability due to the larger range of line strengths (see Section 5.1 for further explanation).
- A very important advantage is that comparison of transitions with positive and negative q_1 coefficients minimizes systematic effects (see Section 5.1.3 in particular).

Finally, we note that the q_1 and q_2 coefficients for Al II $\lambda 1670$ and Si II $\lambda 1526$ in Table 1 have not been presented elsewhere before. In the case of Al II $\lambda 1670$, the coefficients were calculated using the same methods described in Dzuba et al. (1999a,b). The coefficients for Si II $\lambda 1808$ do appear in Dzuba et al. (1999b) but the calculation has been re-performed to include other Si II lines, including $\lambda 1526$. Thus, there is a small ($\approx 5\%$) difference between the previ-

ous value and the one presented in Table 1. This small difference is within the precision of the Dzuba et al. (1999a,b) calculations and does not significantly affect our determination of $\Delta\alpha/\alpha$.

5 DATA REQUIREMENTS, ACQUISITION AND REDUCTION

The fitting of high-resolution (FWHM $\sim 7\text{ km s}^{-1}$, $R \sim 45000$), moderate signal-to-noise ratio (SNR ~ 30 per pixel) QSO absorption lines routinely yields redshifts of single velocity components measured to precisions of $\sigma(z) \sim 3 \times 10^{-6}$ or $\sigma(v) \sim 1\text{ km s}^{-1}$ in velocity space (Outram, Chaffee & Carswell 1999). By comparison with the line shifts in Table 2 and accepting that several well constrained velocity components will exist in each absorption complex, the level of precision achievable with the MM method is $\sigma(\Delta\alpha/\alpha) \sim 10^{-5}$ per absorption cloud. If systematic effects are to be avoided when using a large number (i.e. ~ 50) of absorption systems then, from equation 4, we require ω_0 to be known to a precision of $\sigma(\omega_0) \sim 0.003\text{ cm}^{-1}$ – an order of magnitude more precise than available wavenumber compilations (e.g. Morton 1991).

We therefore require high-resolution, moderate SNR

Table 2. Shift in the rest frame wavenumber, wavelength and velocity space for $\Delta\alpha/\alpha = +10^{-5}$

Transition	$\Delta\omega$ 10^{-2}cm^{-1}	$\Delta\lambda$ 10^{-3}\AA	Δv km s^{-1}
Mg I $\lambda 2853$	0.17	-0.14	-0.015
Mg II $\lambda 2796$	0.42	-0.33	-0.035
Mg II $\lambda 2803$	0.24	-0.19	-0.020
Al II $\lambda 1670$	0.54	-0.15	-0.027
Al III $\lambda 1854$	0.93	-0.32	-0.052
Al III $\lambda 1862$	0.43	-0.15	-0.024
Si II $\lambda 1526$	0.14	-0.032	-0.0062
Si II $\lambda 1808$	1.06	-0.35	-0.058
Cr II $\lambda 2056$	-2.11	0.89	0.130
Cr II $\lambda 2062$	-2.40	1.02	0.148
Cr II $\lambda 2066$	-2.57	1.10	0.159
Fe II $\lambda 1608$	2.57	-0.66	-0.124
Fe II $\lambda 1611$	2.41	-0.63	-0.117
Fe II $\lambda 2344$	2.84	-1.56	-0.199
Fe II $\lambda 2374$	3.56	-2.01	-0.254
Fe II $\lambda 2383$	3.28	-1.86	-0.234
Fe II $\lambda 2587$	3.23	-2.16	-0.250
Fe II $\lambda 2600$	2.91	-1.97	-0.227
Ni II $\lambda 1709$	1.60	-0.47	-0.082
Ni II $\lambda 1741$	-1.50	0.46	0.078
Ni II $\lambda 1751$	-0.80	0.25	0.042
Zn II $\lambda 2026$	4.96	-2.04	-0.301
Zn II $\lambda 2062$	3.15	-1.34	-0.195

QSO spectra and new laboratory measurements of UV resonance transition wavelengths in order to reach a precision of $\sigma(\Delta\alpha/\alpha) \sim 10^{-5}$ for each absorption system.

5.1 QSO Spectra

5.1.1 General properties

All our QSO spectra were obtained at the Keck I 10 m telescope with the HIRES facility (Vogt et al. 1994). The spectra separate conveniently into two samples with several defining features. One sample comprises spectra of 28 Mg II/Fe II absorbers in the spectra of 17 QSOs covering a redshift range $0.5 < z_{\text{abs}} < 1.8$. The second sample comprises 18 damped Lyman- α systems (DLAs) in the spectra of 11 QSOs covering $1.8 < z_{\text{abs}} < 3.5$. This later sample also contains three lower redshift Mg II/Fe II systems (i.e. a total of 21 absorbers comprises this sample). Different groups observed each sample. Thus, with only a small degree of overlap, we label the samples according to the typical redshift of the absorption systems. The major difference between the low- z and high- z samples is that the low- z sample only contains transitions of Mg II and Fe II whereas the high- z sample has a more diverse range of transitions present (see Section 5.1.3).

5.1.2 Low- z ($0.5 < z < 1.8$, $\langle z \rangle = 1.0$)

This sample comprises the same data set analysed in W99, with some differences as detailed in Section 6.1. The observations were taken in 1994 July, 1995 January and 1996 July. The SNR per pixel ranged from 15–50 with most spectra having SNR ~ 30 . The FWHM was $\sim 6.6 \text{ km s}^{-1}$ ($R =$

45000). The QSOs were generally bright ($m_V \lesssim 17.5$) and so several short (~ 1000 s) exposures were taken of each object. The data were reduced with a combination of IRAF[†] routines and personal code. Individual frames were overscan subtracted, bias frame corrected and flatfielded. Cosmic rays were removed by median filtering and the frames were averaged to form the final image. 1σ error arrays were generated assuming Poisson counting statistics. We fitted continua to regions of each spectrum containing any of the relevant transitions by fitting Legendre polynomials to $\sim 500 \text{ km s}^{-1}$ sections. Full details of the reduction process are given in Churchill (1995, 1997) and Churchill et al. (1999). We have also used the spectrum of Q0000–26 analysed by Lu et al. (1996).

Wavelength calibration of the frames was carried out within IRAF: Thorium–Argon (ThAr) lamp exposures were taken before and after the QSO exposures and co-added to provide a calibration spectrum. ThAr lines were selected and centroided to provide a wavelength solution. The solution was applied to the corresponding spectra without any resampling or linearization so that the absorption line shapes were not distorted in the process. We also note that no image rotator was installed during these observations and so the spectrograph slit was not perpendicular to the horizon in general. We make a detailed analysis of these points and their effect on our results in M01b.

The transitions used in this sample are the five Fe lines, Fe II $\lambda 2344$ – $\lambda 2600$, and the Mg transitions, Mg I $\lambda 2853$, Mg II $\lambda 2796$ and $\lambda 2803$. The Mg lines have small q_1 coefficients and so act as anchors against which the larger Fe II shifts can be measured. This set of lines is also very useful because it offers a range of line strengths due to the differing Fe II oscillator strengths (see Table 1) and, together with the similar ionization potentials of Fe II and Mg II, facilitates reliable determination of the velocity structure of the absorption complex. In some cases the Mg II lines are saturated and so the Mg II lines themselves provide only weak constraints on $\Delta\alpha/\alpha$. However, the weak Mg I $\lambda 2853$ then often serves to provide a good constraint on the velocity structure – a further advantage of using Mg/Fe absorption systems to probe $\Delta\alpha/\alpha$. To illustrate these points, we provide an example absorption system, together with our Voigt profile fits, in Fig. 1.

5.1.3 High- z ($0.9 < z < 3.5$, $\langle z \rangle = 2.1$)

These observations were spread over many observing runs from 1994 to 1997. The SNR per pixel ranges from 15–40 with most spectra having SNR ~ 30 and FWHM $\lesssim 7.5 \text{ km s}^{-1}$ ($R = 34000$). The QSOs themselves are at higher redshift and so appear much fainter than those of the low- z sample: $m_V \lesssim 19.0$. Consequently, the total integration times were much longer than for the low- z sample and many more frames were co-added during the reduction process. An image rotator was installed in 1996 August and so only

[†] IRAF is distributed by the National Optical Astronomy Observatories, which are operated by the Association of Universities for Research in Astronomy, Inc., under cooperative agreement with the National Science Foundation.

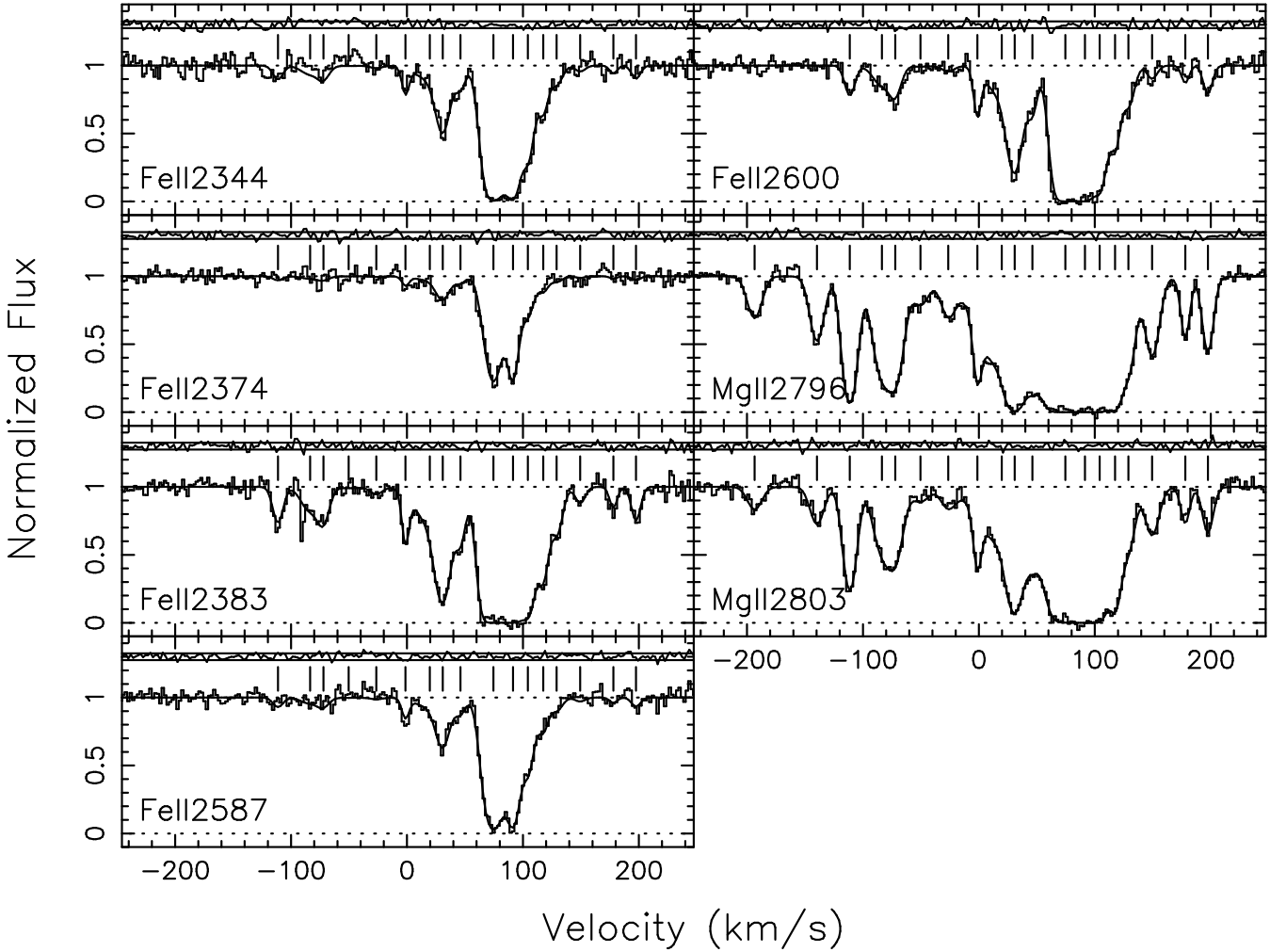


Figure 1. Mg/Fe absorption system towards Q1213–003 at $z = 1.554$. The data have been normalized by a fit to the continuum and plotted as a histogram. Our Voigt profile fit (solid curve) and the residuals (i.e. [data] – [fit]), normalized to the 1σ errors (horizontal solid lines), are also shown. The tick-marks above the continuum indicate individual velocity components. Note the range of line strengths in Fe II, facilitating determination of the velocity structure. The large number of Fe II transitions and the large number of velocity components allows for tight constraints to be placed on $\Delta\alpha/\alpha$. In this case, the Mg I $\lambda 2853$ is also present but is sufficiently weak so as not to provide any constraint on $\Delta\alpha/\alpha$. In cases where the Mg II lines are more saturated, the Mg I line is typically stronger and can be used to constrain the velocity structure.

about half the observations were carried out with the slit perpendicular to the horizon.

Most of the data were reduced using MAKEE, the HIRES data reduction package written by T. Barlow. This package converts the two-dimensional echelle images to fully reduced, one-dimensional, wavelength calibrated spectra (calibration spectra were taken in the same way as for the low- z sample). Some of the spectra were reduced when MAKEE had no wavelength calibration facility. In these cases, wavelength calibration was carried out using IRAF routines. The remainder of the spectra were fully reduced within IRAF. 1σ error arrays were generated assuming Poisson counting statistics. We fitted continua to regions of each spectrum containing any of the relevant transitions by fitting Legendre polynomials to $\sim 500 \text{ km s}^{-1}$ sections. Full details of the reduction procedures can be found in Prochaska & Wolfe (1996, 1997, 1999). Outram, Chaffee & Carswell (1999) have also kindly

provided their spectrum of Q1759+75 which was taken in 1997 July.

We also noted a small but important difference between the IRAF and MAKEE wavelength calibration software. IRAF makes use of an internal list of vacuum ThAr wavelengths and so spectra calibrated with IRAF have “correct” wavelength scales. However, the MAKEE package calibrates spectra with a list of air ThAr wavelengths and converts the final QSO wavelength scale to vacuum using the Cauchy formula for the refractive index (Weast 1979). However, this formula does not reproduce the experimental dispersion: it shows deviations from experiment at the level of 10^{-6} in the optical range. We therefore converted the wavelength scales of the spectra reduced with MAKEE back to air wavelengths using the Cauchy formula and then re-converted to vacuum wavelengths with the preferred Edlén (1966) formula. A detailed discussion of air–vacuum conversion with caveats of the above statements is given in M01b.

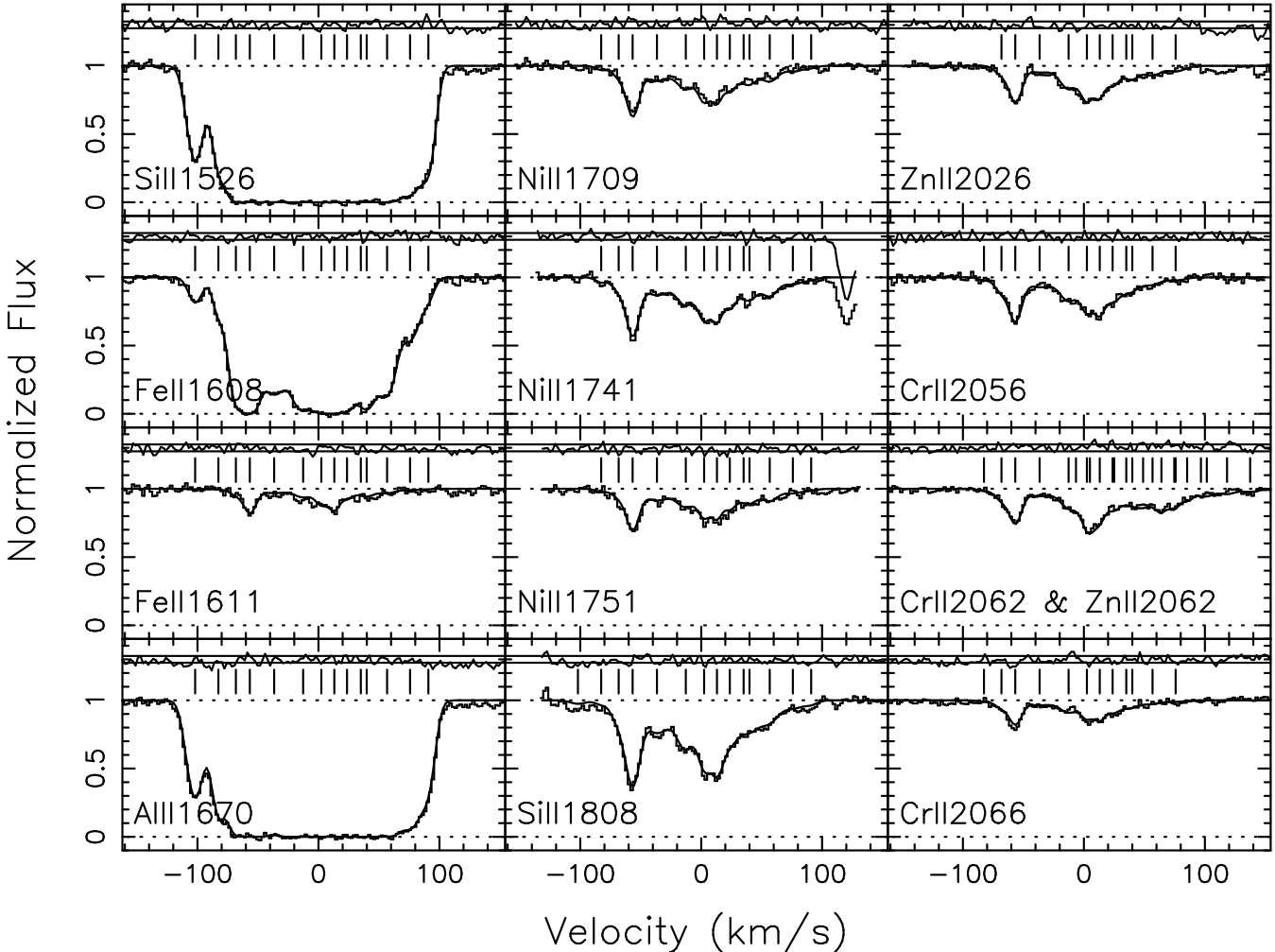


Figure 2. Heavy element absorption lines from the damped Lyman- α system towards Q2206–199 at $z = 1.920$. We illustrate this system since it displays both saturated and unsaturated transitions. However, the metal lines in other DLAs generally have lower column densities. The data have been normalized by a fit to the continuum and plotted as a histogram. Our Voigt profile fit (solid curve) and the residuals (i.e. [data] – [fit]), normalized to the 1σ errors (horizontal solid lines), are also shown. The tick-marks above the continuum indicate individual velocity components. In this case, the Fe II and Si II lines provide constraints on the velocity structure while the Ni II, Cr II and Zn II are strong enough to provide tight constraints on $\Delta\alpha/\alpha$. Note that the Cr II and Zn II $\lambda 2062$ profiles are blended together but that the constraints on the velocity structure from all other transitions allow us to make a statistically acceptable fit.

Theoretically, in damped systems such as those comprising this sample, the combination of lines providing the best constraints on $\Delta\alpha/\alpha$ are those of Zn II and Cr II. In practice, however, these lines are generally quite weak and so the parameter constraints are not optimal. Also, the Zn II and Cr II $\lambda 2062$ profiles are often blended together (the transitions are only separated by 60 km s^{-1}), reducing the strength of the $\Delta\alpha/\alpha$ constraint. The Ni II lines are also generally weak but have the advantage of a variety of widely differing q_1 coefficients. Also note that the only Fe II lines available for these high- z absorbers are the Fe II $\lambda 1608$ and $\lambda 1611$ lines. These can be used in conjunction with the two Si II lines to provide a reasonable constraint on $\Delta\alpha/\alpha$ but their main advantage is that they provide good constraints on the velocity structure. We plot a typical absorption complex in Fig. 2 to illustrate the above points and also to give the reader some idea of the relative strengths of the different transitions used in analysing this sample.

In 6 spectra we have also fitted the two lines of Al III. Variations in the incident radiation field could give rise to changes in the relative column densities when comparing species with ionization potentials above and below the Lyman edge. In our sample, the Al III velocity structures corresponded well with those of the singly ionized atoms (consistent with the conclusions of Wolfe & Prochaska 2000) and the value of $\Delta\alpha/\alpha$ proved to be slightly better constrained by including the Al III lines. In some cases, however, some velocity components in the Al III profiles were much weaker or stronger relative to the other components when compared with the profiles of singly ionized species. In one case, our fitting algorithm removed many weak Al III components from the fit (see Section 6.1) and so we removed the Al III data in this instance.

Table 3. The isotopic structures of the Mg and Si transitions. The composite values are given in Table 1. The Mg isotopic spacings were measured by Hallstadius (1979) but the spacings for Si are estimates based on a scaling of the Mg II $\lambda 2796$ structure. The hyperfine structure of ^{25}Mg is also shown (Drullinger, Wineland & Bergquist 1980). The last column shows the relative abundance of each isotope (Rosman & Taylor 1998). Isotopic information was not used for any heavier ions.

Transition	<i>m</i> /amu	ω_0/cm^{-1}	$\lambda_0/\text{\AA}$	%
Mg I $\lambda 2853$	24	35051.271	2852.9636	79.0
	25	35051.295	2852.9616	10.0
	26	35051.318	2852.9598	11.0
Mg II $\lambda 2803$	24	35669.286	2803.5324	79.0
	25	35669.300	2803.5313	2.7
	25	35669.310	2803.5305	1.5
	25	35669.360	2803.5266	2.8
	25	35669.370	2803.5258	3.0
	26	35669.388	2803.5244	11.0
Mg II $\lambda 2796$	24	35760.835	2796.3553	79.0
	25	35760.853	2796.3539	4.2
	25	35760.913	2796.3492	5.8
	26	35760.937	2796.3473	11.0
Si II $\lambda 1808$	28	55309.330	1808.0132	92.2
	29	55309.390	1808.0113	4.7
	30	55309.446	1808.0094	3.1
Si II $\lambda 1526$	28	65500.442	1526.7073	92.2
	29	65500.517	1526.7055	4.7
	30	65500.583	1526.7040	3.1

5.2 Laboratory wavelength measurements

The laboratory rest wavelengths were measured by various groups using Fourier transform spectrometry. We discuss the measurements for each ion below, concentrating on those issues most relevant to our analysis. We present the wavelengths that we have adopted in Table 1. It is interesting to note that, with the exception of the Fe II spectrum, the wavelengths presented in Table 1 are systematically longer than those compiled in Morton (1991) – a widely used list of resonance transition wavelengths. For a particular transition, the wavelengths are generally consistent but, taken altogether, a systematic trend is noted.

- Mg I and Mg II: These spectra have recently been measured by Pickering, Thorne & Webb (1998). The spectra of Ni I and Ni II were excited along with those of Mg I and Mg II and several of these lines were used for calibration. The Ni I spectrum of Litzén, Brault & Thorne (1993) was used for reference which itself was calibrated from the Fe I and Fe II lines of Nave et al. (1991). The Mg II $\lambda 2796$ wavelength has been measured previously by Drullinger, Wineland & Bergquist (1980) and Nagourney & Dehmelt (1981) and the wavenumbers are in excellent agreement. Also, a confirmation of the Pickering et al. (1998) wavenumbers has been made and is described briefly in Pickering et al. (2000).

Since Mg is a relatively light atom, the isotopic structure of the line profile must be taken into account. Pickering et al. (1998) used the isotopic spacings measured by Hallstadius (1979) to obtain absolute wavelengths for the isotopes. These values are listed in Table 3 and were used in our analysis.

- Si II, Al II and Al III: These spectra have recently been measured by Griesmann & Kling (2000). The C IV and Si IV spectra were also measured and all spectra were calibrated using the Ar II spectrum of Whaling et al. (1995). At present, there are no other similarly precise measurements of these spectra.

To our knowledge, the isotopic spacings for the Si II transitions have not been measured. The mass shift and the specific mass shift should dominate the volume shift in such a light ion. The $\lambda 1526$ transition is very similar to those of Mg II and so the specific mass shift should be of the same order. Thus, to estimate the isotopic spacings in Si II $\lambda 1526$ we have scaled the spacings of Mg II $\lambda 2796$ by the mass shift: $\Delta\omega_i \propto \omega_0/m^2$ for $\Delta\omega_i$ the wavenumber shift for a given isotope *i* where *m* is the atomic mass. We have used these spacings to fit a synthetic Gaussian emission line (centred at the composite wavelength) in order to estimate the absolute wavenumbers for the isotopes. We present the results in Table 3. We performed similar calculations for the Si II $\lambda 1808$ transition. However, the assumption that the specific shift for $\lambda 1808$ is similar to that for the Mg II transitions is not so justified in this case since the transitions are of quite different type (see Table 1). We discuss any effect this approximation may have on $\Delta\alpha/\alpha$ in M01b but find that it should be negligibly small.

- Cr II and Zn II: These spectra have been measured independently using two different Fourier transform spectrometers: one at Imperial College (IC), and another at Lund University (LU). The two experiments are described in Pickering et al. (2000). The wavenumber calibration was based on the Fe I and II standards of Nave et al. (1991) in both cases.

- Fe II: This spectrum, from 1750–3850 \AA , is presented in Nave et al. (1991). The wavelength calibration was done by comparison with the Norlén (1973) Ar II spectrum. No other (similarly precise) catalogues of Fe II lines exist in the literature. We have obtained the Fe II $\lambda 1608$ and $\lambda 1611$ wavenumbers from S. Johansson (private communication).

- Ni II: This spectrum was recently measured by Pickering et al. (2000). The original spectra were measured during the Mg I and II experiments by Pickering et al. (1998). Wavenumber calibration was done using the Ni II standards of Litzén, Brault & Thorne (1993) which cover the region down to about 2000 \AA . The Ni I lines between 1750 \AA and 2000 \AA were calibrated with the Fe I and II lines so as to be used as calibration lines for the Ni II spectrum. R. Kling (private communication) has confirmed these wavenumbers, albeit with lower precision.

All wavelength calibrations above rely on the the Ar II spectrum measured by either Norlén (1973) or Whaling et al. (1995). However, the Norlén and Whaling calibrations systematically disagree. The Whaling wavenumbers are larger and the difference between them is proportional to the wavenumber: $\delta\omega = 7 \times 10^{-8}\omega$. Since this difference is linear in frequency (velocity) space, as long as we normalize all measured wavenumbers to the one calibration scale, any systematic error will be completely absorbed into the redshift parameter when we centroid corresponding velocity components in different transitions in the absorption systems (see Section 6.1 for further explanation). We choose to normalize all measured wavenumbers to the Norlén calibra-

tion scale and so the wavelengths of the Si II, Al II and Al III transitions in Table 1 have been scaled accordingly.

Also of note is that we only take into account the isotopic structures for the lightest two elements, Mg and Si. In the optically thin limit, the centroids of the isotopic structures described in Table 3 reduce to the composite values given in Table 1. When a line becomes optically thick, differential saturation of the isotopic components causes the centroid of the composite line to shift. This effect is discussed in detail in M01b and it is evident that we do not need to include isotopic information for the heavier ions.

6 ANALYSIS AND RESULTS

6.1 Analysis

Our analysis technique is based on a simultaneous χ^2 minimization analysis of multiple component Voigt profile fits to the absorption features in several different transitions. Consider a QSO spectrum containing a single velocity component of a specific transition. Three parameters describe the Voigt profile fit to such a component: the column density, the Doppler width or b -parameter and the redshift z of the absorbing gas cloud. In our case, however, each absorption system contains many blended velocity components appearing in many different transitions.

The central assumption in the analysis is that the velocity structure seen in one ion corresponds exactly to that seen in any other ion. That is, we assume that there is negligible proper motion between corresponding velocity components of all ionic species. With this assumption comes a reduction in the number of free parameters to be varied in a particular fit since the redshift of corresponding velocity components in different transitions need only be specified once. We discuss this assumption and any effect it may have on $\Delta\alpha/\alpha$ in M01b.

Further restrictions can be placed on the number of free parameters when fitting different transitions simultaneously since the b -parameters of corresponding velocity components in different ionic species are physically related. We may write

$$b_i^2 = \frac{2kT}{M_i} + b_{\text{turb}}^2 \quad (6)$$

as the b -parameter of an ionic species i which has a mass M_i . The first term describes the thermal broadening within a gas cloud which has a kinetic temperature, T , and the second term describes an additional turbulent motion which affects all ions equally. If we assume that either thermal or turbulent broadening dominates for a particular component then again we reduce the number of free parameters. If we fit transitions of at least two ions with different masses then we can determine T and b_{turb} for each velocity component.

For the present case, we wish to add another free parameter to the fit: $\Delta\alpha/\alpha$. From equation 4 we can see that $\Delta\alpha/\alpha$ will be constrained by the difference $\omega_z - \omega_0$ for each transition if we fit two or more transitions simultaneously[§].

[§] We require two or more transitions since fitting only one would render z and $\Delta\alpha/\alpha$ degenerate for a single component and nearly degenerate for multiple components.

We have used the program VPFIT[¶] (Webb 1987) to fit absorption profiles to the spectra. Previously, VPFIT did not allow one to vary T and b_{turb} for each component independently, but dealt only with b_i . There was also no provision for including $\Delta\alpha/\alpha$ as a free parameter. We have therefore modified VPFIT to include T , b_{turb} and $\Delta\alpha/\alpha$ explicitly as free parameters. This differs from the analysis in W99 where $\Delta\alpha/\alpha$ was varied externally to VPFIT. The main advantage is a significant gain in computational speed, allowing us to fit more complicated systems that would have taken prohibitively long using the method in W99. A minor point is that W99 presented 30 absorption systems whereas we present 28 using the same QSO spectral data due to slightly different subdivision of neighbouring absorption complexes.

Parameter errors can be calculated from the diagonal terms of the final parameter covariance matrix (Fisher 1958). The reliability of these errors has been confirmed using Monte Carlo simulations of a variety of different combinations of transitions and velocity structures.

VPFIT imposes a cut-off point in parameter space such that very weak velocity components are removed from the fit when they no longer significantly affect the value of χ^2 . This presents a problem for our method since a given component may be weak in one transition (and so can be regarded as dispensable with respect to χ^2) but may be strong in another. An example of this can be seen in Fig. 2 where the two lowest velocity components do not appear in the weaker transitions. Conceivably, dropping even very weak components could affect our determination of $\Delta\alpha/\alpha$. Therefore, in such cases we observed the trend in the values of $(\Delta\alpha/\alpha)_i$ at each iteration i of the minimization routine to see if this trend was significantly altered due to line dropping. If components were dropped during a fit then we also re-ran the VPFIT algorithm, keeping the dropped components by fixing their column density at the value just before they were dropped from the original fit. No cases were found where the values of $\Delta\alpha/\alpha$ from the different runs differed significantly.

We impose several consistency checks before we accept a value of $\Delta\alpha/\alpha$. Firstly, the value of χ^2 per degree of freedom must be ~ 1 . Secondly, to check internal consistency, we make three different fits to the data with three different conditions on the b -parameters: (i) entirely thermal broadening, (ii) entirely turbulent broadening and (iii) a fit where T and b_{turb} are determined by goodness of fit. The values of $\Delta\alpha/\alpha$ derived from the three fits should be consistent with each other since the choice above should not greatly affect $\Delta\alpha/\alpha$ (i.e. the redshifts of velocity components will not change systematically). If this was not the case then the system was rejected. Only 2 systems were rejected in this way. Since (iii) is the most physically realistic choice we expect χ^2 for that fit to be less than that for cases (i) and (ii). This was indeed the case for all but a few systems. These exceptions were found to have very low average temperatures (across the velocity structure) or very small values of b_{turb} . The difference between χ^2 for the fit for case (iii) and (ii) or (i) respectively was small in these cases. We selected the final value of $\Delta\alpha/\alpha$ from the regime which gave the lowest χ^2 but the results were insensitive to this choice.

[¶] See <http://www.ast.cam.ac.uk/~rfc/vpfit.html> for details about obtaining VPFIT.

6.2 Results

We have analysed the low- z sample in two stages. The first was motivated by the fact that we have used different techniques to those of W99. We took the final velocity structures for each absorption system found by W99, used them as first guesses for the parameters and determined $\Delta\alpha/\alpha$ with our new methods. In all cases the results were nearly identical to those of W99. The second stage was to fit the entire data set again, using no information about previous velocity structures. These are the results we present below.

Our results are presented in Table 4. We give the object, the QSO emission redshift, z_{em} , the absorption cloud redshift, z_{abs} , $\Delta\alpha/\alpha$ for that cloud and its associated 1σ error. The transitions for each cloud are indicated with the ID letters defined in Table 1. Table 5 shows the weighted mean, $\langle\Delta\alpha/\alpha\rangle_w$, the unweighted mean, $\langle\Delta\alpha/\alpha\rangle$ and the significance level, δ , of the weighted mean for the low and high redshift samples and for the sample as a whole. We also include the value of the reduced χ^2 , χ^2_{red} (i.e. χ^2 per degree of freedom), for each sample where the model is taken to be a constant equal to $\langle\Delta\alpha/\alpha\rangle_w$.

Our results show that $\Delta\alpha/\alpha$ deviates from zero at a significance level of 4.1σ over the redshift range $0.5 < z < 3.5$. We also see a general consistency between the low and high- z samples. The values of χ^2_{red} in Table 5 are all less than unity. This indicates that, if we have miscalculated the error bars systematically, we have probably overestimated rather than underestimated them. This is also reflected in a comparison of the root-mean-square deviation from the mean, RMS, and the average size of our error bars, $\langle\sigma(\Delta\alpha/\alpha)\rangle$: for the sample as a whole, $\text{RMS} = 1.46 \times 10^{-5}$ and $\langle\sigma(\Delta\alpha/\alpha)\rangle = 2.01 \times 10^{-5}$. The RMS is also less than $\langle\sigma(\Delta\alpha/\alpha)\rangle$ for the low and high- z samples taken alone. Assuming we have overestimated the errors on $\Delta\alpha/\alpha$ then we can scale them by a constant factor, S , so as to force $\chi^2_{\text{red}} = 1$. Column 8 in Table 5 shows the resulting increase in the significance of $\langle\Delta\alpha/\alpha\rangle_w$. Note that the weighted means do not differ significantly from the unweighted means for either sample suggesting that the data error bars are reliable.

We have also conducted an F test on the $\Delta\alpha/\alpha$ parameter. We used the final velocity structures from the fitting procedure above to re-fit the absorption systems after removing the $\Delta\alpha/\alpha$ parameter. If $\Delta\alpha/\alpha$ is necessary to describe the data then we expect χ^2 for each system to reduce when we include $\Delta\alpha/\alpha$. The reduction should be in accordance with the statistical significance of $\Delta\alpha/\alpha$ for each system. We denote χ^2 for the fit to system i with and without the $\Delta\alpha/\alpha$ parameter as $\chi^2_{\alpha i}$ and $\chi^2_{\alpha' i}$ respectively. If the significance (in units of σ) of the value of $\Delta\alpha/\alpha$ for that system is δ_i , we expect that

$$\sum_i^M (\chi^2_{\alpha' i} - \chi^2_{\alpha i}) = \sum_i^M \delta_i^2 \quad (7)$$

for M absorbers.

The δ_i^2 can be derived from the last column of Table 4. Direct calculation of both sides of equation 7 yields the results in the final two columns of Table 5. $\sum_i (\chi^2_{\alpha i} - \chi^2_{\alpha' i}) \gtrsim \sum_i \delta_i^2$ for both the low and high- z samples, consistent with $\Delta\alpha/\alpha$ being a required parameter.

To illustrate the distribution of $\Delta\alpha/\alpha$ over cosmological time, we plot our results in Fig. 3. The upper panel of

Table 4. The raw results from the χ^2 minimization procedure. For each QSO sight line we identify the QSO emission redshift, z_{em} , the absorption cloud redshift, z_{abs} , the transitions utilized in our analysis and the value of $\Delta\alpha/\alpha$ for each absorption cloud.

Object	z_{em}	z_{abs}	Transition ^a	$\Delta\alpha/\alpha/10^{-5}$
low- z sample				
0000-26	4.11	1.434 ^b	bcqr	-0.732 ± 2.283
0002+05	1.90	0.851	bcnopqr	-0.239 ± 1.516
0117+21	1.49	0.729	abcqr	-0.403 ± 1.298
		1.048	bcnpr	-1.171 ± 1.800
		1.325	bcpqr	0.314 ± 0.765
		1.343	cnpq	-0.982 ± 0.868
0420-01	0.915	0.633	abcr	3.360 ± 5.532
0450-13	2.25	1.175	bnopr	-2.590 ± 0.831
		1.230	bcnpqr	-1.112 ± 0.798
		1.232	bcp	0.611 ± 2.475
0454+03	1.34	0.860	acnopqr	0.007 ± 1.266
		1.153	bcnpqr	-0.340 ± 2.047
0823-22	0.91 ^c	0.911	bcnpqr	-0.068 ± 0.661
1148+38	1.30	0.553	bcqr	-1.882 ± 1.699
1206+45	1.16	0.928	bcnopqr	-0.800 ± 1.578
1213-00	2.69	1.320	abcnopqr	-1.821 ± 0.893
		1.554	bcnopqr	-0.965 ± 0.968
1222+22	2.05	0.668	bcnpr	-0.245 ± 1.549
1225+31	2.22	1.795	abcnopr	-1.473 ± 1.521
1248+40	1.03	0.773	bcnopqr	1.398 ± 1.260
		0.855	bcnpqr	-0.329 ± 1.301
1254+04	1.02	0.519	abcqr	-4.486 ± 4.308
		0.934	bcnpqr	0.530 ± 2.146
1317+27	1.01	0.660	bcnpqr	0.348 ± 1.781
1421+33	1.91	0.843	bcnopqr	-0.111 ± 0.793
		0.903	bcnpqr	-1.093 ± 2.101
		1.173	bcnpr	-2.837 ± 1.807
1634+70	1.34	0.990	bcnpqr	-1.586 ± 3.752
high- z sample				
0019-15	4.53	3.439	ghl	0.920 ± 3.520
0149+33	2.43	2.140	defghijklmstu	-3.420 ± 1.800
0201+37	2.49	1.476	cnoqr	-0.775 ± 0.878
		1.956	ehkl	-0.444 ± 3.243
		2.325	deghl	3.473 ± 2.414
		2.457	dgl	0.902 ± 3.754
		2.462	ghkltu	0.520 ± 1.110
0841+12	2.20 ^c	2.375	dghijtuvw	0.285 ± 3.670
		2.476	dghijklmtu	-1.351 ± 3.052
1215+33	2.61	1.999	defghijklmtuvw	-0.972 ± 3.411
1759+75	3.05	2.625	eghklmstu	-2.199 ± 1.521
		2.625 ^d	dglmstu	-0.354 ± 1.613
2206-20	2.56	0.948	bcnpqr	-2.436 ± 1.724
		1.017	abcnopqr	-0.372 ± 0.689
		1.920	dghijklmstuvwxyz	0.929 ± 1.040
2230+02	2.15	1.858	dghjlnprstu	-1.615 ± 1.699
		1.864	ghijklmnostuvwxyz	-1.376 ± 0.706
2231-00	3.02	2.066	ghjlkmtuvwxyz	-1.590 ± 1.265
2348-14	2.94	2.279	ghl	-0.244 ± 5.204
2359-09	2.31	2.095	dghijklstuvwxyz	-0.946 ± 0.601
		2.154	dfgl	-3.101 ± 6.211

^aTransitions identified as in Table 1.

^bThis absorber taken from Lu et al. (1996).

^cThese QSOs are BL Lac objects and so their emission redshifts have large uncertainties. Indeed, the literature values for z_{em} shown here are less than the measured absorption redshifts.

^dThis absorber contributed by Outram, Chaffee & Carswell (1999).

Table 5. Statistics for the two subsamples and the sample as a whole. We give the average redshift, \bar{z} , for each sample and for the number of data points, N , contributing to the weighted mean, $\langle \Delta\alpha/\alpha \rangle_w$, and unweighted mean, $\langle \Delta\alpha/\alpha \rangle$ (in units of 10^{-5}). We also give the significance, δ , of the deviation from zero and the reduced χ^2 for the weighted mean. $\delta_{\chi^2_{\text{red}}=1}$ is the significance when we force $\chi^2_{\text{red}} = 1$ by scaling all errors on $\Delta\alpha/\alpha$ by S . The final two columns contain the results of the F test.

Sample	\bar{z}	N	$\langle \Delta\alpha/\alpha \rangle_w$	$\langle \Delta\alpha/\alpha \rangle$	δ	χ^2_{red}	$\delta_{\chi^2_{\text{red}}=1}$	S	$\sum_i (\chi^2_{\alpha i} - \chi^2_{\alpha i})$	$\sum_i \delta_i^2$
Low z	1.02	28	-0.70 ± 0.23	-0.67 ± 0.27	3.0σ	0.70	3.6σ	0.84	55	28
High z	2.12	21	-0.76 ± 0.28	-0.67 ± 0.33	2.8σ	0.68	3.3σ	0.83	37	21
Total	1.49	49	-0.72 ± 0.18	-0.67 ± 0.21	4.1σ	0.68	4.9σ	0.83	92	49

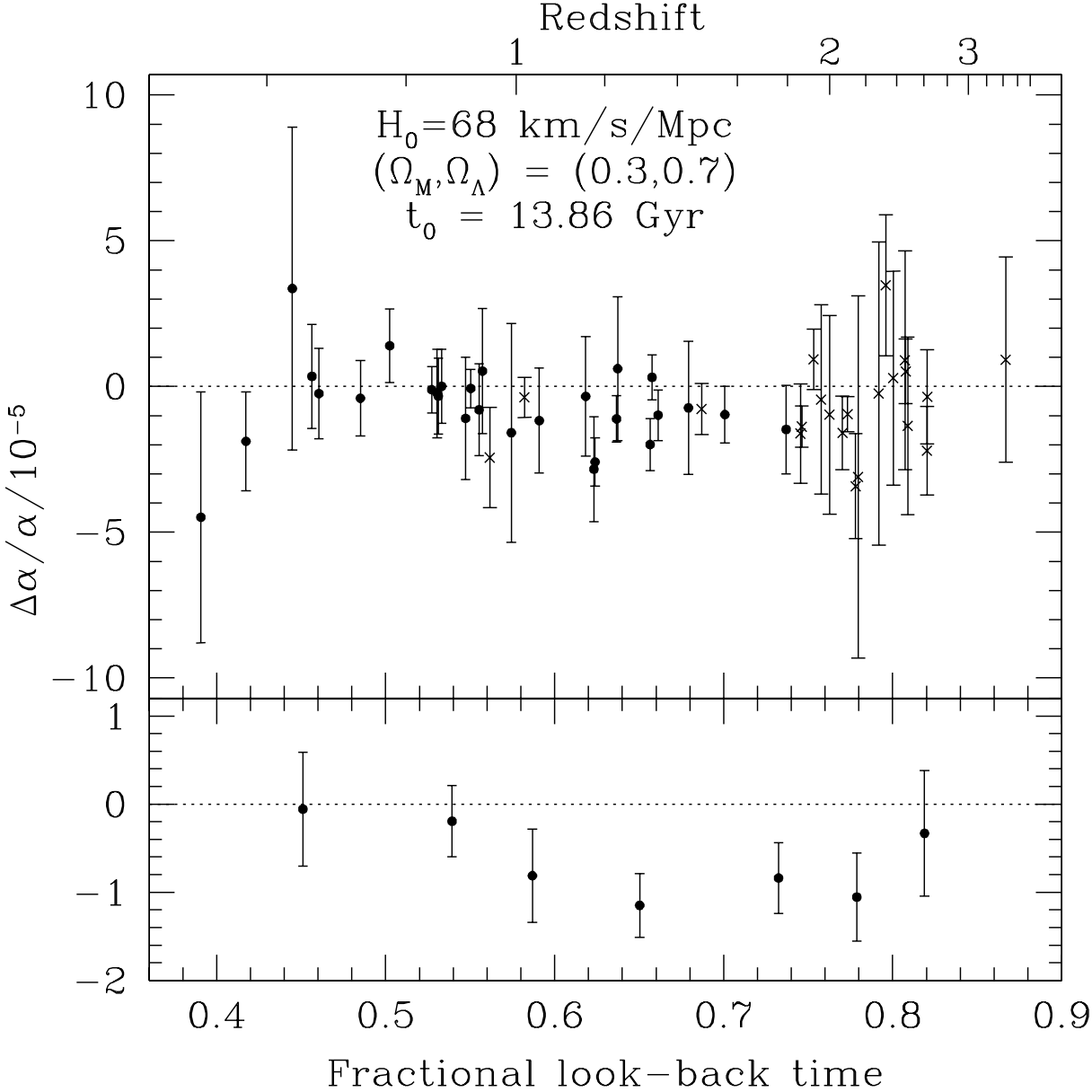


Figure 3. $\Delta\alpha/\alpha$ versus fractional look-back time for a currently popular cosmology. The upper panel shows our raw results and 1σ error bars: the dots represent the low- z sample and the crosses mark the high redshift sample. Note that the high- z sample does contain some lower redshift absorbers. The lower panel shows an arbitrary binning of our results: 7 bins \times 7 points per bin = 49 points. The redshifts of the points are taken as the mean redshift of clouds within that bin and the value of $\Delta\alpha/\alpha$ is the weighted mean with its associated 1σ error bar.

Fig. 3 shows the raw values of $\Delta\alpha/\alpha$ as a function of fractional look-back time to the absorbing cloud using a flat Λ dominated cosmology ($H_0 = 68 \text{ km s}^{-1} \text{Mpc}^{-1}$, $\Omega_M = 0.3$, $\Omega_\Lambda = 0.7$). The redshift scale is also given for comparison. The lower panel shows an arbitrary binning of the data such that all bins have equal number of points (7 bins \times 7 points per bin = 49 points). We plot the weighted mean for each bin with the associated 1σ error bars. At low redshifts we see that $\Delta\alpha/\alpha$ is consistent with zero. Also, the results are consistent with a generally monotonic evolution of α with redshift.

6.3 Systematic errors

The statistical error in our result is now small and our attention must turn to possible systematic errors. In the companion paper, M01b, we explore in detail a broad range of potential systematic errors, including the following: laboratory wavelength errors, wavelength mis-calibration, atmospheric dispersion effects, unidentified interloping transitions, isotopic ratio and/or hyperfine structure effects, intrinsic instrumental profile variations, spectrograph temperature variations, heliocentric velocity corrections, kinematic effects and large scale magnetic fields. All but two of these are shown to be negligible: atmospheric dispersion effects and isotopic abundance variation. In this Section we summarise these two effects, but first discuss how a general wavelength scale distortion effects the low- z and high- z samples differently.

6.3.1 Effect of a distortion of the wavelength scale

To explain our results in terms of an effect other than real variation of α , such an effect must be able to mimic a non-zero average value of $\Delta\alpha/\alpha$ for both the high and low- z samples alike. Generally, simple systematic effects might cause low-order distortions in the wavelength scale (relative to the ThAr calibration frames) or may lead to wavelength dependent mis-centroiding of absorption features.

The low- z sample (Mg II/Fe II systems) is most sensitive to systematic effects. The Fe II lines have large and positive q_1 coefficients and all lie at lower wavelengths than the Mg II anchors. Thus, a systematically negative $\Delta\alpha/\alpha$ can result from a slight ‘compression’ of the QSO spectra relative to the ThAr calibration frames for the low- z sample. However, it is more difficult to understand the effect of simple systematic errors on the high- z sample for several reasons:

- (i) The transitions involved have a large range of q_1 coefficients. In effect, there are three types of transition: those with large and positive q_1 , those with large and negative q_1 and those with small or intermediate values of q_1 .
- (ii) The different types of transition are mixed in wavelength space. In the low- z sample, all the lines with large and positive q_1 (i.e. Fe II lines) lie to the blue of those with small q_1 (i.e. Mg II lines). This is not the case in the high- z sample. For example, two lines with small q_1 , Si II $\lambda 1526$ and Al II $\lambda 1670$, straddle two lines with large, positive q_1 , Fe II $\lambda 1608$ and $\lambda 1611$.
- (iii) Different sets of transitions appear in each QSO spectrum. Some spectra may not contain all types of transition.

The value of $\langle\Delta\alpha/\alpha\rangle_w$ will be more resistant to systematic errors in the high- z sample. To illustrate this point we have ‘compressed’ the spectrum of a low- z and a high- z absorption system by a factor of 1×10^{-5} (i.e. the separation between any two wavelengths decreases by 1 part in 10^5) and found a new value for $\Delta\alpha/\alpha$. We used the same first-guess velocity structures used to derive the results in Table 1 and Fig. 3. For the low- z Mg/Fe system at $z = 0.911$ we find a significant decrease in $\Delta\alpha/\alpha$ due to the compression: $\Delta\alpha/\alpha = (-0.068 \pm 0.661) \times 10^{-5} \rightarrow (-1.106 \pm 0.692) \times 10^{-5}$. However, for the high- z DLA at $z = 2.095$ we find a small, *positive* change: $\Delta\alpha/\alpha = (-0.946 \pm 0.601) \times 10^{-5} \rightarrow (-0.821 \pm 0.589) \times 10^{-5}$.

6.3.2 Atmospheric dispersion effects

Atmospheric dispersion across the spectral direction of the spectrograph slit can be avoided using an image rotator. However, as we noted in Sections 5.1.2 and 5.1.3, many of our objects were observed before HIRES was fitted with an image rotator. Dispersion across the slit can only lead to a ‘stretching’ of the QSO spectrum relative to the ThAr frames. However, at least in the low- z sample, a negative value of $\Delta\alpha/\alpha$ can only be mimicked by a ‘compression’ of the spectrum. The effect of the stretching on $\Delta\alpha/\alpha$ is not quite as clear for the high- z sample (points (i)–(iii) above).

We quantify the atmospheric dispersion effects in M01b and find that the high- z sample is quite robust against this error. However, the low- z results are more sensitive to this effect and may have to be *reduced* from the uncorrected value of $\langle\Delta\alpha/\alpha\rangle_w = (-0.70 \pm 0.23) \times 10^{-5}$ to $\langle\Delta\alpha/\alpha\rangle_w \approx (-1.52 \pm 0.23) \times 10^{-5}$. We stress that the magnitude of the correction here is an upper limit since several effects, all difficult to properly quantify, will act to reduce the effective compression. Note that since the above correction is an upper limit, we do not include any additional errors due to uncertainties in our model of atmospheric refraction.

6.3.3 Isotopic abundance evolution

We assumed terrestrial isotopic abundances in all species when fitting the QSO spectra. However, if the isotopic abundances in the QSO absorbers are different, small apparent shifts in the absorption lines would be introduced, potentially mimicking a non-zero $\Delta\alpha/\alpha$. $\Delta\alpha/\alpha$ is most sensitive to changes in the isotopic abundances of Mg II and Si II since these ions have large isotopic separations (see Section 5.2). Timmes, Woosley & Weaver (1995), Timmes & Clayton (1996) and Gay & Lambert (2000), suggest that the abundances of the isotopes $^{25,26}\text{Mg}$ and $^{29,30}\text{Si}$ decrease with decreasing metallicity. The QSO absorption clouds in our sample have low metallicity compared to solar (Prochaska & Wolfe 1999, 2000; Churchill et al. 1999). Thus, to obtain an upper limit on the effect this may have had on $\Delta\alpha/\alpha$, we have removed the $^{25,26}\text{Mg}$ and $^{29,30}\text{Si}$ isotopes from our analysis and re-calculated $\Delta\alpha/\alpha$ for all the absorption systems. Again, we find that the correction is towards more negative values, the corrected value being $\Delta\alpha/\alpha = (-0.96 \pm 0.17) \times 10^{-5}$ (as in Section 6.3.2, we do not add any additional errors due to uncertainties in our model since the correction we calculate is an upper limit).

6.3.4 Tests for unknown, simple systematic errors

We have also carried out other tests to search for any unknown, simple systematic effects. For example, it is unlikely that such an effect will be able to mimic the very specific q_1 dependence of the transitions in the high- z sample. Thus, if we remove the transitions with large, positive q_1 coefficients from our fit and find a new value for $\Delta\alpha/\alpha$, we expect the two values to differ if the line shifts are caused by some simple systematic effect. Of course, if we remove transitions with large, positive q_1 , we can only obtain useful constraints on $\Delta\alpha/\alpha$ if anchor lines *and* transitions with large, negative q_1 are available. Therefore, we have conducted such a test on a subset of the high- z sample which contains at least one anchor line, at least one transition with large and positive q_1 and at least one with large and negative q_1 . We find consistent weighted mean values of $\Delta\alpha/\alpha$ both before and after line removal. We conducted a similar test by removing lines with large, negative q_1 and another test by removing the anchor lines. We find consistent values before and after line removal in each case. Thus, the interpretation that the line shifts we observe are caused by a varying α seems robust.

7 DISCUSSION

We have conducted an experimental search for variability of α over the redshift range $0.5 < z < 3.5$ using QSO absorption lines as our probe. We used a new method for deriving constraints on $\Delta\alpha/\alpha$ from a comparison of QSO and laboratory spectra which, unlike the previous alkali-doublet (spin-orbit splitting) method, exploits the total relativistic effect in different atoms (see Section 4). Comparing the wavelengths of transitions from different multiplets and different atoms/ions leads to an order of magnitude gain in precision over the alkali-doublet (AD) method. Since the new, many-multiplet (MM) method allows us to use all transitions in principle, we also gain precision through increased statistics.

We have analysed the spectra of 49 absorption clouds (towards 28 QSOs) and compared the observed and laboratory wavelengths of those transitions listed in Table 1. Our low- z results represent a re-analysis of the W99 data. We compare the W99 results with our re-analysis in Table 6 and we see that they are consistent. Our results for each absorption system are listed in Table 4. Over the entire sample we find statistical evidence for time variation of α at the 4.1σ level: $\Delta\alpha/\alpha = -0.72 \pm 0.18$ (see Table 5). This result is the ‘raw’ result. Correcting for any possible systematic effects (Section 6.3 and M01b) would *increase* the significance of this deviation of $\Delta\alpha/\alpha$ from zero. We show the distribution of $\Delta\alpha/\alpha$ with cosmological time and redshift in Fig. 3.

From the analyses we present in this paper and in M01b, we conclude that if our results are due to some effect other than a real variation in α , this will only be revealed by further independent observations and analyses using the MM method. Optical spectra are very useful for probing the range of redshifts we have explored here. However, a statistical sample of radio spectra of H I 21 cm and molecular absorption systems has the potential to increase our precision limit by another order of magnitude. This effort is hampered by the fact that very few such systems are known at present. A systematic observational search for these systems

Table 6. Comparison of results from W99 and the present work (low- z sample only) in different redshift regimes. Values of $\Delta\alpha/\alpha$ are given in units of 10^{-5} .

	Redshift range		
	$z < 1.0$	$z > 1.0$	$0.5 < z < 1.8$
Webb et al. (1999)	-0.2 ± 0.4	-1.9 ± 0.5	-1.1 ± 0.4
This paper	-0.2 ± 0.3	-1.2 ± 0.3	-0.70 ± 0.23

should clearly be made. Also, as the arsenal of 8–10 m class optical telescopes with high-resolution spectrographs grows, more observations should be devoted to obtaining carefully calibrated, high SNR spectra of absorption systems at both high and low- z . These will provide a crucial check on our results and will allow us to discover or rule out any further subtle or unknown systematic effects in the data.

ACKNOWLEDGMENTS

We are very grateful to Ulf Griesmann, Sveneric Johansson, Rainer Kling, Richard Learner, Ulf Litzén, Juliet Pickering and Anne Thorne for conducting laboratory wavelength measurements especially for the present work and for communicating their results prior to publication. We would also like to thank Michael Bessell, Tom Bida, Bob Carswell, Rolf Engleman Jr., Alberto Fernández-Soto, John Hearnshaw, Alexander Ivanchik, Jochen Liske, Leon Lucy, Geoff Marcy, Gillian Nave and Steve Vogt for very helpful communications. We are grateful to the John Templeton Foundation for supporting this work. MTM and JKW are grateful for hospitality at the IoA Cambridge, where some of this work was carried out. JDB acknowledges support from PPARC, The Royal Society, and a Gordon Godfrey visiting professorship at UNSW. AMW received partial NSF support from NSF grant AST0071257.

REFERENCES

Albrecht A., Magueijo J., 1999, Phys. Rev. D, 59, 043516
 Antoniadis I., Arkani-Hamed N., Dimopoulos S., Dvali G., 1998, Phys. Lett. B, 436, 257
 Arkani-Hamed N., Dimopoulos S., Dvali G., 1998, Phys. Lett. B, 429, 263
 Avelino P. P., Martins C. J. A. P., Rocha G., 2000, Phys. Lett. B, 483, 210
 Bahcall J. N., Sargent W. L. W., Schmidt M., 1967, ApJ, 149, L11
 Barrow J. D., 1987, Phys. Rev. D, 35, 1805
 Barrow J. D., 1990, in Bertotti B., Balbinot R., Bergia S., Messina A., eds., Modern Cosmology in Retrospect, Cambridge University Press, Cambridge, p. 67
 Barrow J. D., 1999, Phys. Rev. D, 59, 043515
 Barrow J. D., Magueijo J., 1998, Phys. Lett. B, 443, 104
 Barrow J. D., Magueijo J., 1999a, Phys. Lett. B, 447, 246
 Barrow J. D., Magueijo J., 1999b, Class. Q. Gravity, 16, 1435
 Barrow J. D., Magueijo J., 2000, ApJ, 532, L87
 Barrow J. D., O’Toole C., 2001, MNRAS, 322, 585
 Barrow J. D., Tipler F. J., 1996, The Anthropic Cosmological Principle, Oxford University Press, Oxford, UK

Battye R. A., Crittenden R., Weller J., 2001, Phys. Rev. D, 63, 043505

Bekenstein J. D., 1982, Phys. Rev. D, 25, 1527

Bergeson S. D., Lawler J. E., 1993, ApJ, 408, 382

Bergström L., Iguri S., Rubinstein H., 1999, Phys. Rev. D, 60, 045005

Brans C., Dicke R. H., 1961, Phys. Rev., 124, 924

Campbell B. A., Olive K. A., 1995, Phys. Lett. B, 345, 429

Cardelli J. A., Savage B. D., 1995, ApJ, 452, 275

Carilli C. L. et al., 2000, Phys. Rev. Lett., 85, 5511

Carroll S. M., 1998, Phys. Rev. Lett., 81, 3067

Chamoun M., Landau S. J., Vucetich H., 2001, Phys. Lett. B, 504, 1

Chandrasekhar S., 1937, Nat, 139, 757

Chodos A., Detweiler S., 1980, Phys. Rev. D, 21, 2167

Churchill C. W., 1995, Lick Technical Report #74

Churchill C. W., 1997, PhD thesis, UC Santa Cruz

Churchill C. W., Rigby J. R., Charlton J. C., Vogt S. S., 1999, ApJS, 120, 51

Cowie L. L., Songaila A., 1995, ApJ, 453, 596

Damour T., Dyson F. J., 1996, Nucl. Phys. B, 480, 37

Damour T., Polyakov A. M., 1994, Nucl. Phys. B, 423, 532

Dicke R. H., 1957, Rev. Mod. Phys., 29, 355

Dicke R. H., 1961, Nat, 192, 440

Dirac P. A. M., 1937, Nat, 139, 323

Drinkwater M. J., Webb J. K., Barrow J. D., Flambaum V. V., 1998, MNRAS, 295, 457

Drullinger R. E., Wineland D. J., Bergquist J. C., 1980, Appl. Phys., 22, 365

Dufton P. L., Hibbert A., Kingston A. E., Tully J. A., 1983, MNRAS, 202, 145

Dzuba V. A., Flambaum V. V., Webb J. K., 1999a, Phys. Rev. Lett., 82, 888

Dzuba V. A., Flambaum V. V., Webb J. K., 1999b, Phys. Rev. A, 59, 230

Dzuba V. A., Flambaum V. V., Murphy M. T., Webb J. K., 2001, Phys. Rev. A, 63, 042509

Edlén B., 1966, Metrologia, 2, 71

Fedchak J. A., Lawler J. E., 1999, ApJ, 523, 734

Fisher R. A., 1958, Statistical methods for research workers, Harper, New York, USA

Forgács P., Horváth Z., 1979, General Relativity and Gravitation, 10, 931

Freund P., 1982, Nucl. Phys. B, 209, 146

Fujii Y., Iwamoto A., Fukahori T., Ohnuki T., Nakagawa M., Hidaka H., Oura Y., Möller P., 2000, Nucl. Phys. B, 573, 377

Gamow G., 1967, Phys. Rev. Lett., 19, 913

Gay P. L., Lambert D. L., 2000, ApJ, 533, 260

Griesmann U., Kling R., 2000, ApJ, 536, L113

Haldane J. B. S., 1937a, Nat, 139, 1002

Haldane J. B. S., 1937b, Nat, 158, 555

Hallstadius L., 1979, Z. Phys. A, 291, 1220

Hannestad S., 1999, Phys. Rev. D, 60, 023515

Hill C. T., Ross G. G., 1988a, Nucl. Phys. B, 311, 253

Hill C. T., Ross G. G., 1988b, Phys. Lett. B, 203, 125

Hill C. T., Steinhardt P. J., Turner M. S., 1980, Phys. Lett. B, 252, 343, 1990

Hořava P., Witten F., 1996a, Nucl. Phys. B, 460, 506

Hořava P., Witten F., 1996b, Phys. Rev. D, 54, 7561

Jordan P., 1937, Naturwiss., 25, 513

Jordan P., 1939, Z. Physik, 113, 660

Kaplinghat M., Scherrer R. J., Turner M. S., 1999, Phys. Rev. D, 60, 023516

Kaluza T., 1921, Preuss. Akad. Wiss. K, 1, 966

Klein O., 1926, Z. Phys., 37, 895

Kolb E. W., Perry M. J., Walker T. P., 1986, Phys. Rev. D, 33, 869

Kothari D. S., 1938, Nat, 142, 354

Kujat J., Scherrer R. J., 2000, Phys. Rev. D, 62, 023510

Landau L. D., 1955, in Pauli W., ed., Neils Bohr and the Development of Physics, McGraw-Hill, NY, p. 52

Li L. -X., Gott J. R. III, 1998, Phys. Rev. D, 58, 103513

Litzén U., Brault J. W., Thorne A. P., 1993, Phys. Scr., 47, 628

Livio M., Stiavelli M., 1998, ApJ, 507, L13

Lu L., Sargent W. L. W., Womble D. S., Takada-Hidai M., 1996, ApJ, 472, 509

Maeda K. I., 1988, Mod. Phys. Lett. A, 3, 242

Magueijo J., 2000, Phys. Rev. D, 62, 103521

Marciano W. J., 1984, Phys. Rev. Lett., 52, 489

Milne E. A., 1935, Relativity, Gravitation and World Structure, Clarendon press, Oxford

Milne E. A., 1937, Proc. Roy. Soc. A, 158, 324

Moffatt J., 1993, Int. J. Mod. Phys. D, 2, 351

Morton D. C., 1991, ApJS, 77, 119

Murphy M. T., Webb J. K., Flambaum V. V., Churchill C. W., Prochaska J. X., 2001b, MNRAS, accepted (M01b) (astro-ph/0012420)

Murphy M. T., Webb J. K., Flambaum V. V., Prochaska J. X., Wolfe A. M., 2001c, MNRAS, accepted (astro-ph/0012421)

Murphy M. T., Webb J. K., Flambaum V. V., Drinkwater M. J., Combes F., Wiklund T., 2001d, MNRAS, accepted (astro-ph/0101519)

Nagourney W., Dehmelt H. G., 1981, Bull. Am. Phys. Soc., 26, 805

Nave G., Learner R. C. M., Thorne A. P., Harris C. J., 1991, J. Opt. Soc. Am. B, 8, 2028

Norlén G., 1973, Phys. Scr., 8, 249

Outram P. J., Chaffee F. H., Carswell R. F., 1999, MNRAS, 310, 289

Pagel B. E. J., 1983, Phil. Trans. Roy. Soc. A, 310, 245

Perlmutter S. et al., 1999, ApJ, 517, 565

Pickering J. C., Thorne A. P., Webb J. K., 1998, MNRAS, 300, 131

Pickering J. C., Thorne A. P., Murray J. E., Litzén U., Johansson S., Zilio V., Webb J. K., 2000, MNRAS, 319, 163

Prestage J. D., Robert L. T., Maleki L., 1995, Phys. Rev. Lett., 74, 3511

Prochaska J. X., Wolfe A. M., 1996, ApJ, 470, 403

Prochaska J. X., Wolfe A. M., 1997, ApJ, 474, 140

Prochaska J. X., Wolfe A. M., 1999, ApJS, 121, 369

Prochaska J. X., Wolfe A. M., 2000, ApJ, 533, L5

Randall L., Sundrum R., 1999a, Phys. Rev. Lett., 83, 3370

Randall L., Sundrum R., 1999b, Phys. Rev. Lett., 83, 4690

Rosman K. J. R., Taylor P. D. P., 1998, Pure and Applied Chemistry, 70, 217

Savedoff M. P., 1956, Nat, 178, 689

Schmidt B. P. et al., 1998, ApJ, 507, 46

Shlyakhter A. I., 1976, Nat, 25, 340

Teller E., 1948, Phys. Rev., 73, 801

Timmes F. X., Clayton D. D., 1996, ApJ, 472, 723

Timmes F. X., Woosley S. E., Weaver T. A., 1995, ApJS, 98, 617

Varshalovich D. A., Panchuk V. E., Ivanchik A. V., 1996, Astron. Lett., 22, 6

Varshalovich D. A., Potekhin A. Y., 1996, Astron. Lett., 22, 1

Varshalovich D. A., Potekhin A. Y., Ivanchik A. V., 2000, in Dunford R. W., Gemmel D. S., Kanter E. P., Kraessig B., Southworth S. H., Young L., eds., AIP Conf. Proc. 506, X-ray and Inner-Shell Processes. Argonne National Laboratory, Argonne, Illinois, p. 503

Verner D. A., Verner E. M., Ferland G. J., 1996, At. Data Nucl. Data Tables, 64, 1

Vogt S. S. et al., 1994, in Crawford D. L., Craine E. R., eds., Instrumentation in Astronomy VIII, SPIE, 2198, 362

Weast R. C., 1979, Handbook of Chemistry and Physics (60th edition), CRC Press, Florida, p. E-387

Webb J. K., 1987, PhD thesis, Cambridge University

Webb J. K., Flambaum V. V., Churchill C. W., Drinkwater M. J., Barrow J. D., 1999, Phys. Rev. Lett., 82, 884 (W99)

Webb J. K., Murphy M. T., Flambaum V. V., Dzuba V. A., Barrow J. D., Churchill C. W., Prochaska J. X., Wolfe A. M., 2001, Phys. Rev. Lett., accepted (astro-ph/0012539)

Whaling W., Anderson W. H. C., Carle M. T., Brault J. W., Zarem H. A., 1995, J. Quant. Spectrosc. Radiat. Transfer, 53, 1

Wolfe A. M., Brown R. L., Roberts M. S., 1976, Phys. Rev. Lett., 37, 179

Wolfe A. M., Prochaska J. X., 2000, ApJ, 545, 603

Wu Y., Wang Z., 1986, Phys. Rev. Lett., 57, 1978